ANALYSIS OF THE VELOCITY DISTRIBUTION AT THE BLADE TIPS OF AXIAL-FLOW COMPRESSORS

H. Ufer
Fried. Krupp GmbH Central Institute for Research and Development, Essen

Translation of "Analyse der Geschwindigkeitsverteilung an den Schaufelspitzen von Axialgebläsen"
Technische Mitteilungen Krupp (Forschungsberichte), Vol. 26, No. 2, Oct. 1968, pp. 33-45.

(NASA-TT-F-16366) ANALYSIS OF THE VELOCITY DISTRIBUTION AT THE BLADE TIPS OF AXIAL-FLOW COMPRESSORS (Kanner (Leo) Associates) 27 p
CSCL 21E
N75-22319
Unclas
G3/07 19478

NATIONAL AERONAUTICS AND SPACE ADMINISTRATION
WASHINGTON, D. C. 20546 MAY 1975

STANDARD TITLE PAGE

1. Report No. NASA TT F-16366	2. Government Accession No.	3. Recipient's Catalog No.
4. Title and Subtitle ANALYSIS OF THE VELOCITY DISTRIBUTION AT THE BLADE TIPS OF AXIAL-FLOW COMPRESSORS		5. Report Date May 1975 6. Performing Organization Code
7. Author(s) H. Ufer		8. Performing Organization Report No. 10. Work Unit No.
9. Performing Organization Name and Address Leo Kanner Associates, P.O. Box 5187, Redwood City, California 94063		11. Contract or Grant No. NASw-2481 13. Type of Report and Period Covered Translation
12. Sponsoring Agency Name and Address National Aeronautics and Space Administration, Washington D. C. 20546		14. Sponsoring Agency Code

15. Supplementary Notes
Translation of "Analyse der Geschwindigkeitsverteilung an den Schaufelspitzen von Axialgebläsen," Technische Mitteilungen Krupp (Forschungsberichte), Vol. 26, No. 2, Oct. 1968, pp. 33-45.

16. Abstract Velocity distribution at the blade tips of axial-flow compressors is analyzed on the basis of measurements and calculations; it is found that clearance flow has direct effect on flow at blade tips as well as indirect effect on flow as far as the hub. Good qualitative agreement was found between flow at stationary rectilinear cascades and at rotating cascades.

17. Key Words (Selected by Author(s))	18. Distribution Statement
	Unclassified-Unlimited

19. Security Classif. (of this report)	20. Security Classif. (of this page)	21.
Unclassified	Unclassified	

ANALYSIS OF THE VELOCITY DISTRIBUTION AT THE BLADE TIPS OF AXIAL-FLOW COMPRESSORS

H. Ufer[1]

1. Introduction

/33*

In most jet engines with an axial construction there is a clearance between the rotating blade and the housing wall through which the pressure differential on the blade tips can be equalized between the suction and pressure sides. A flow is created through the clearance (clearance flow), which flows tranverse to the main flow direction and is included in the secondary flows in the impeller. It disturbs the flow in the impeller and causes changes in the local pressure on the blades and leads to changes in the lift and the resistance, changes in the direction of the fluid streaming from the blade passages and, thereby, to a worsening of the effective capacity of the jet engine.

The problem of clearance flow is difficult to surmount both through calculation and experiment. The primary flow processes take place close to the walls so that measurements with normal pressure probes are hardly possible. The problem seems even more opaque analytically, since the combined effects of the secondary flow yields a very confused three-dimensional flow field in the blade and side wall boundary layers and the clearance flow. Very steep velocity and pressure gradients as well as strong direction changes appear.

Since the clearance flow also appears in a frictionless, incompressible flow and the flow processes at the blade ends can be described through the use of the third Helmholtz vorticity theorum as with a finite airfoil wing, the description of the flow phenomenon begins with this conception. Through numerous experimental studies

---

[1]This study was undertaken at the Hermann-Fottinger Institute of the Technical University of Berlin within the framework of the research project "Hot Wire Measurements in a Rotating System" of the German Research Association, under the direction of Prof. Dr.-Ing. C. Schreck.
* Numbers in the margin indicate pagination in the foreign text.

with stationary individual blades or cascades [1 through 6] it was ascertained that the observed flow behavior at the blade tips could not be explained with this idealized model, since actual fluids (cf. Fig. 1), have, in part, opposing directions along the blades. This flow property takes place in the flow around the blades in proximity to the clearance, since the boundary layers of the blades, especially on the suction side, are strongly affected. In the jet engine, the clearance wall at the impeller moves relative to the blade. In a turbine cascade the relative movement of the clearance wall is directed form the suction to the pressure side, i.e., against the direction of the clearance flow (Fig. 2). Because of the viscosity of the flowing medium it pulls the particles immediately present on the wall against the flow direction through the clearance and, in this way, works against the clearance flow. In the compressor grid the relative movement of the clearance wall is directed from the blade pressure side to the blade suction side, whereby the clearance flow is aided (Fig.2).

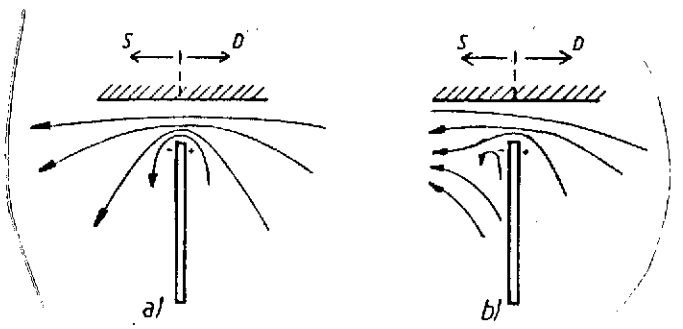

Fig. 1. Schematic representation of the flow procedure at the clearance.
a) for ideal fluid
b) for fluids encountering friction
S = suction side
D = pressure side

A series of experimental studies on the problem of clearance flow is already well known, in which, however, the border conditions of the problem is usually simplified. All previous studies were concerned with measurements of static cascade which were either level or a star type impeller. The relative movement of the housing wall was replaced by a revolving band in many cases [1, 3, 4, 5]. The question of whether these results can be applied to rotating cascade remain unanswered. There are studies [7-9], in which the translation of results from level to stationary band cascades

/34

for a few cases was tested and the problem of how these results could be translated to rotating cascades was considered, but, nonetheless, it was not shown whether or not the same flow processes take place on rotating cascades as are observed on stationary level or fanned cascades.

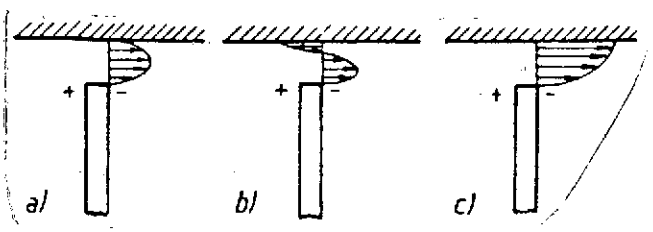

Fig. 2. Course of clearance flow in turbine and compressor cascades; viewed by an observer rotating with the cascades.
a) without wall movement
b) with wall movement in a turbine
c) with wall movement in a compressor

Measurements behind the axial compressor impellers [10 through 13] which spatially bound probs in proximity to the blade tips allow unexpectedly large deflections, buoyancy coefficients and losses. The boundary layer of the housing wall often climbs up to 20% of the blade height behind the impellers. The percentage of such a boundary layer thickening which could be attributed to the clearance flow has not been experimentally clarified. The hypothesis [13] that the thickening of the boundary layer at the side wall is based on the centrifuged blade boundary level, which is deflected in the axial direction has not been experimentally tested.

In the present work an attempt is made to analyze the flow processes at the blade tips in a rotating axial flow-through cascade by velocity measurements in the moving system. We hope to show to what extent the course of the velocities in the blade passages, immediately after blade discharge and over the entire blade height it is effected by clearance flow. A comparison to these studies of a static, flat ~~grid~~ will show whether or not a rotating cascade has the same flow processes and effects as a stationary cascade.

2. Experiment Arrangement

2.1 Experimental Cascade

The experiment was performed with a axial ventilator impeller. This had full profile blades, the camber lines of which were circular

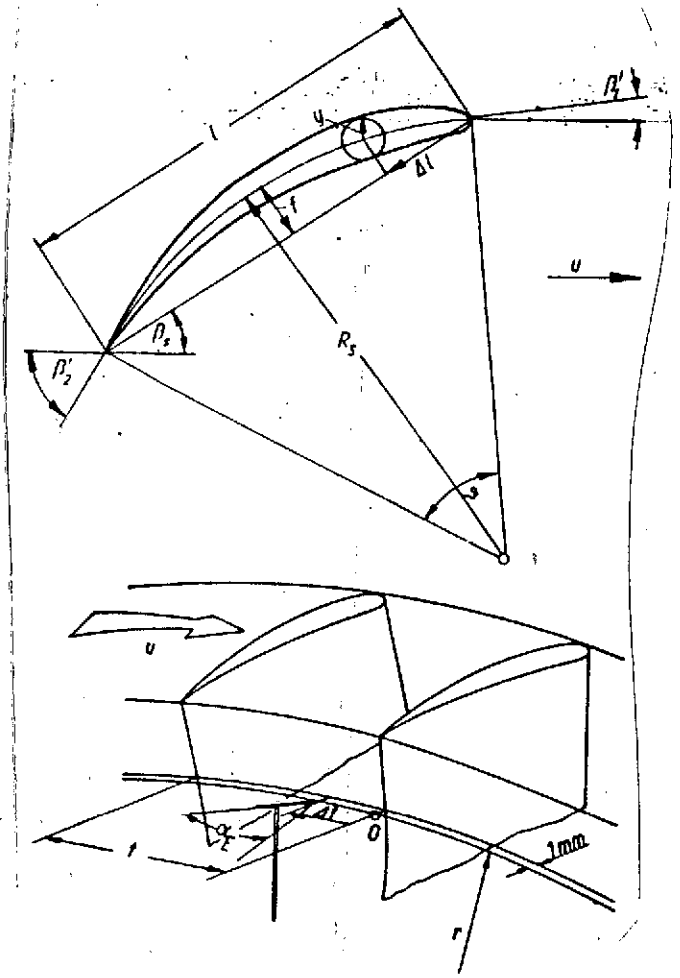

Fig. 3. Blade geometry and probe coordinates, f = maximum camber of the airfoil section, ℓ = airfoil length, Δℓ = coordinates in the direction of the cord line, Rs = circumference radius, r = radius of the cylinder section, t = blade section, Δt = coordinates in the perimeter direction, u = perimeter velocity, y = airfoil section thickness, α_E = angle of incidence of the probe from the axial direction, β_s = stagger angle, β'_1 = blade inlet angle, β'_2 = blade discharge angle, θ = blade circumference angle.

arcs. The secondary ratio was 0.63. The blading was set for constant spin for the production of a flow behind the impeller. A guide wheel with 14 skeleton blades, which directed the flow in the axial direction.

Fig. 3 shows the blade geometry and probe coordinates and Fig. 4 gives the blade parameters for the impeller and guide wheel. The designation of the velocity components and the angle in the mobile and stationary systems are given in Fig. 5. Since the probes rotate between the impeller and the guide wheel, the guide wheel must be removed 0.5 times the diameter in the axial direction for the measurement. The diameter of the impeller housing D is 400 mm and the clearance with s between the impeller and the housing is 1 mm. Related to the blade height h the clearance with s/h = 1.35%. Fig. 6 shows the characteristic curve for the impeller with its guide wheel. The pressure coefficient ψ_t at the stagger angle at the blade point β_{sa} = 25° is plotted against the flow coefficient ϕ. At this point the operating level with the greatest efficiency is reached. Δp_t is the total pressure at the

measuring point 1 (Fig. 7). It is calculated from the measured static pressure and the dynamic pressure calculated from the volume flow V. The density ρ of the flow medium can be, therefore, assumed to be constant throughout the entire region, since the flow velocity is continually smaller than 50 m/s and the pressure differences were smaller than 100 kp/m^2.

In this dimensionless depiction the characteristic curve is independent of the number of revolutions and the diameter of the impeller as long as the Reynolds number and Mach number do not change significantly.

2.2 Test Stand

For the experiment the impeller was built into a test stand for axial ventilators (Fig. 7). It sucked in air from the experiment room through a known rotating inlet jet and conveys it in a tubing, which serves as a measurement section for the measurement of the pressure increase and the flow volume as well as the throttling. /35 The torque on the impeller shaft was determined with a swivel-bearing motor. The number of revolutions of the impeller were 2000/min in each measurement. It was maintained at ± 1% constant through electronic regulation.

3. Measurement Technique

As was said above the studies of the clearance flow on static cascades met serious measurement technical difficulties. For measurements of rotating cascades the problems of measurement translation and probe adjustment and maintenance are also factors. Since primarily the clearance flow and its effects must be investigated phenomenologically, i.e. the force of the velocities must be determined, the hot wire measurement technique was seen as especially suitable here. It has the great advantage over the technique with pressure probes that the measurement values can be translated electrically from the rotating system. Further, velocity variations can be measured up to

frequencies of 80 kHz. In this way, the absolute flow through the individual blade passages and the turbulent variations can also be measured with a static probe. These variations can be seen as exchange motion between the boundary layers of the housing wall and the blades, the clearance flow and the undisturbed flow and allows the region of strong mixture of these various flows and their boundaries. Since the hot wire anemometer can be very small, there is no significant disturbance of flow. /36

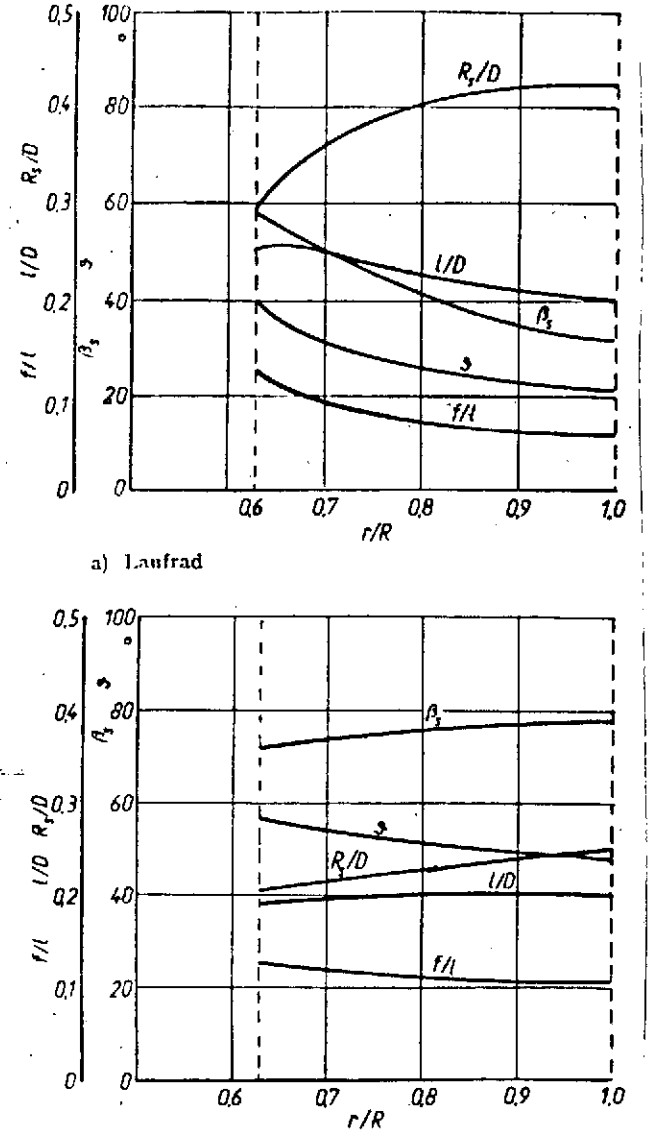

a) Laufrad

Fig. 4. Blade parameters for the impeller and guide wheel related to the outer diameter D plotted against the radius ratio r/R (cf. Fig. 3).

Key: a) impeller b) guide wheel

For the measurement of the rotating system a measurement apparatus was developed which is depicted in Fig. 8 along with the impeller. It can be disassembled as a whole from the impeller to the calibrator of the probes. Fig. 9 shows the hot wire measurement apparatus with various probe holders.

3.1 Direction Measurements with Hot Wire Anemometer

For the measurements of the flow velocity and the flow direction probes with monofilament hot wires were used. The varying heat flow in the hot wire, when this flowed in different directions to its length axis -- in extreme cases transverse or along its axis -- velocity readings dependent upon the flow direction were given. This difficult property was used for direction measurements.

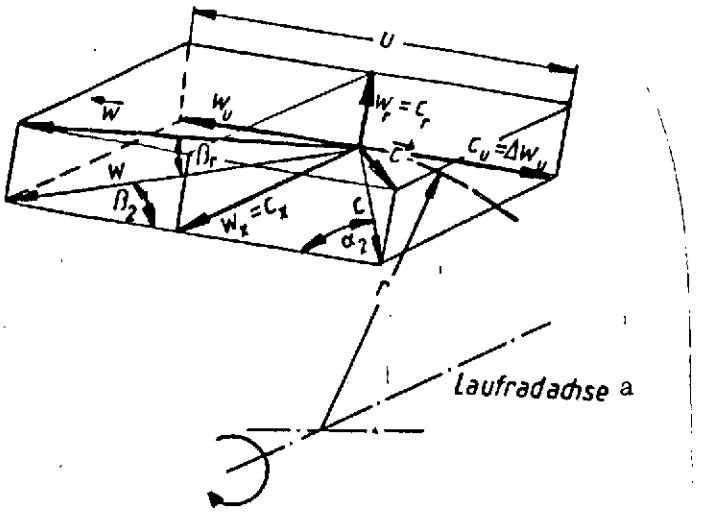

Fig. 5. Representation of the velocity components and angles in a mobile and a static frame of reference $\vec{c}$ = vector of the absolute velocity, c_r = radial component, c_u = parameter component, c = absolute velocity in the cylinder section surface, $\vec{w}$ = vector of the relative velocity, w_r = the radial components, w_u = circumferential components, w_x = axial components, w = relative velocity in the cylinder section surface, Δw_u = deflection of the relative velocity, α_2 = angle of absolute velocity c against the circumferential direction, β_2 = angle of the relative velocity w against the circumference direction, β_r = angle of the vector of relative velocity w against the cylinder surface.

Key: a. impeller axis

Since the direction characteristic of a hot-wire anemomter is dependent upon the form of the probe prong, the hot-wire length and the hot-wire setting between the prongs, a few probe forms were investigated in the pretest The attempt was made to develop a hot-wire anemometer which could measure the velocity independent of the flow direction and was highly sensitive to the direction. These properties were satisfactorily filled by the hot-wire anemometer shown in Fig. 10[2].

The probes were comprised of platinum-iridium tublets with a 1.3 mm outer diameter and 0.8 mm inner diameter. The prongs were of 0.6 mm thick nickel wire. The hot-wire itself is a platinum wire of 5 µm diameter and about 2.5 mm long. It was attached to the prongs by spot welding.

In Fig. 11 the direction dependence of the velocity recorder of the probes is depicted for the two vertical planes. The angles of incidence and slide, γ and ε, were determined according to Fig. 12.

[2]The form of the probe prongs was developed by Dipl.-Ing. K. Giese of the Hermann Föttinger Institute for flow technology of the Technical University of Berlin.

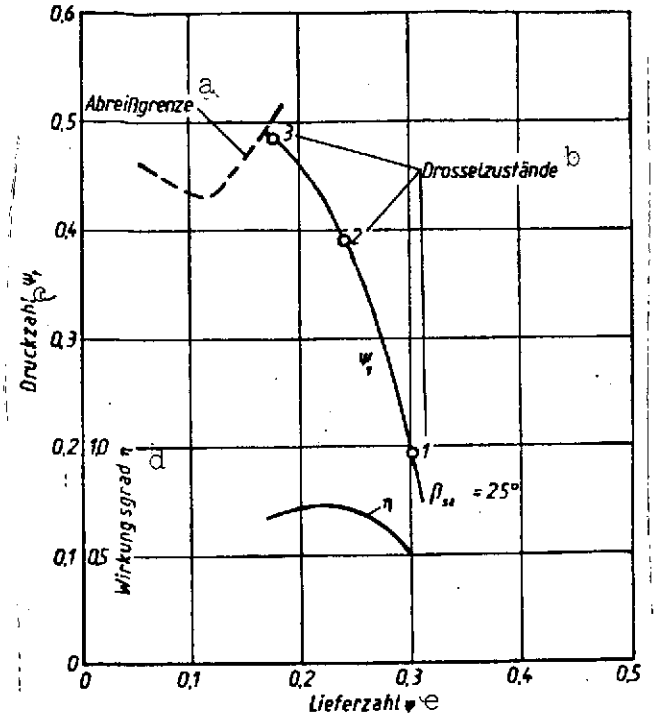

Fig. 6. Characteristic curve of the ventilator.

A $\varphi = \frac{4\dot{V}}{\pi D^2 u_a}$ = flow coefficient

B $\psi_t = \frac{\Delta p_t}{(\rho/2) u_a^2}$ = pressure coefficient

C $\eta = \frac{\Delta p_t \dot{V}}{N_W}$ = efficiency

D = impeller radius, β_{sa} = stagger angle at the blade tips, u_a = circumferential velocity at the outer diameter, N_W = lift performance of the axle, = total pressure increase, $\dot{V}$ = volume flow, ρ = density.

Key: a. limit for disruption of flow
b. thrusting condition
c. pressure coefficient
d. efficiency
e. flow coefficient

With this probe the velocity can be measured in the direction insensitive positive and the direction can be measured in the other position. It can be seen that in the region /37 of zero flow direction the direction sensitivity is small. Therefore, a probe was developed which is direction sensitive for this region. A small glass cylinder was fixed between the prongs of the probe and the hot-wire was fastened parallel to this. This lie immediately (0.1 mm) before the cylinder about which the flow passed and continually measured a velocity based upon the flow about the cylinder. The direction behavior of this probe (cf. Fig. 10, below) is depicted in Fig. 13.

3.2 Methods for Direction Determination

The method by which the flow direction was determined depended upon the velocity in the tangential and radial directions [14]. The method which measured primarily the velocity at the discharge of the cascade determined the amount

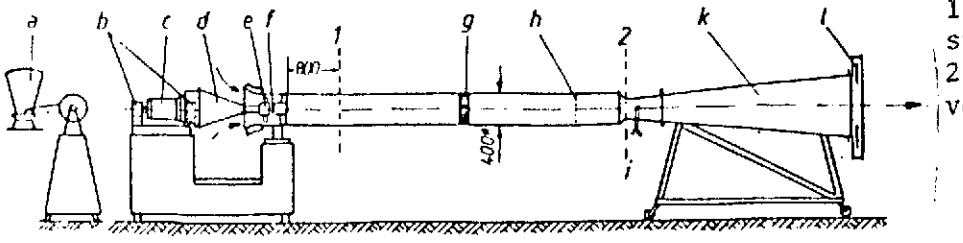

1 Point of measurement for static pressure
2 Point of measurement for volume flow V

Fig. 7. Schematic representation of the experiment arrangement, a-propeller torque, b-air suspension, c-swivel bearing motor, d-bearing housing, e-test wheel, f-co-rotational hot-wire anemometer, g-straightener, h-screen, i-nozzle, k-diffuser, l-iris diaphragm.

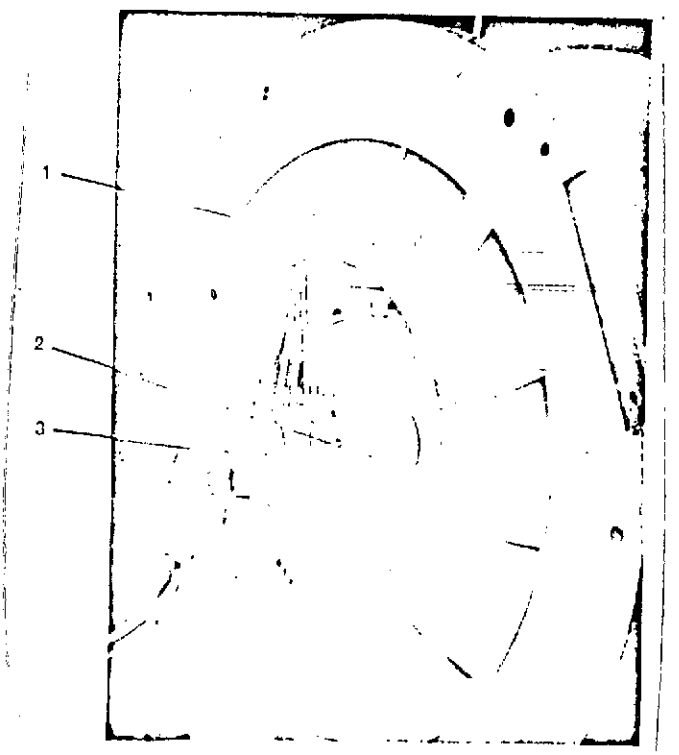

Fig. 8. Hot-wire measurement apparatus in a rotating system 1 probe holder, 2 probe adjustment mechanism, 3 rotation transducer.

of relative velocity with a co-rotational probe and the amount of absolute velocity with a stationary probe.

With a given radial /38
velocity the velocity triangle can be designated from which the radial and axial components of the flow can be taken. The hot-wire is in a radial direction for these measurements and the probes are placed approximately in the flow direction. To determine the radial components the hot-wire direction anemometer shown in Fig. 10 was used. If the probe was placed in the impeller so that the axis of

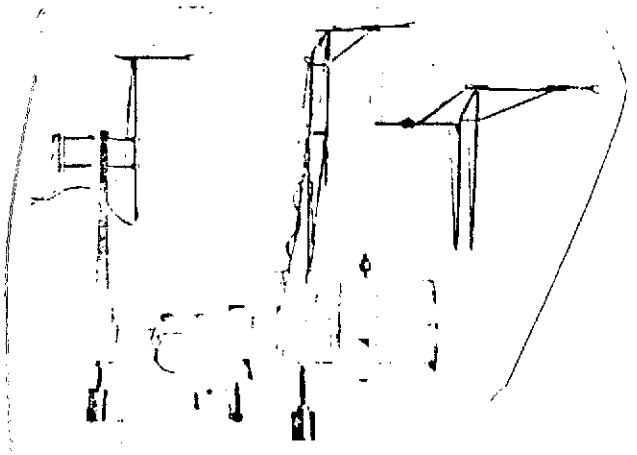

Fig. 9. Hot-wire measurement aparratus with various probe holders.

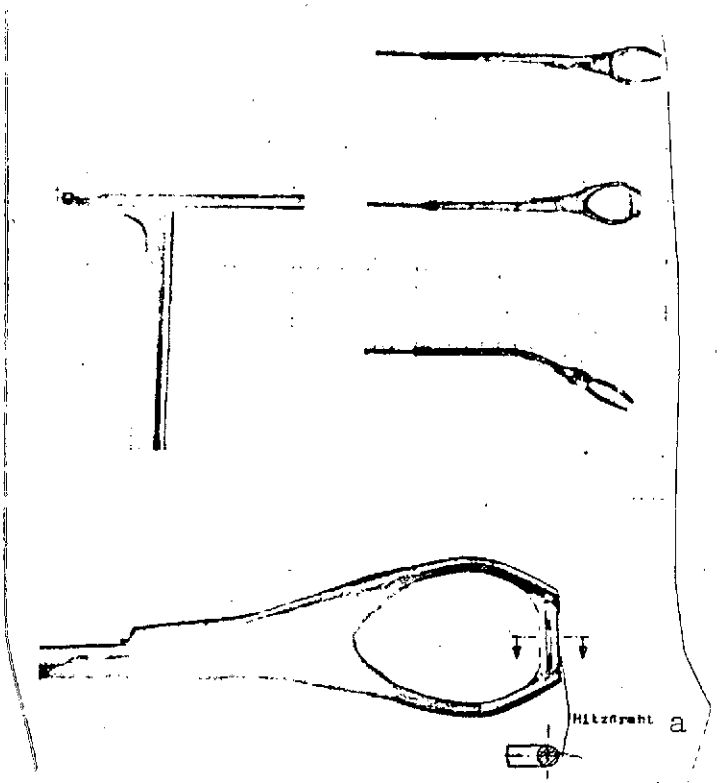

Fig. 10. Hot-wire anemometer forms below: hot-wire direction probe, magnified approximately 4 times.

Key: a. hot wire

its hot-wire was tangential to the cylinder section surface and the flow reached this surface at an angle, then this is equivalent to an incident flow at angle γ according to Fig. 12. According to Fig.12 large velocity changes are shown with small deviations from the zero direction. In this way even small direction deviations of the flow from the cylinder section surface, which depicts the flow plane in the impeller, i.e., the radial flow components can be determined. In order to determine this positive or negative direction two measurements with the probe must be performed. The second measurement must be rotated 180° from the first measurement about the probe shaft. According to the flow direction, the velocity of the first measurement is larger or smaller than the second in the asymetrical calibration curve.

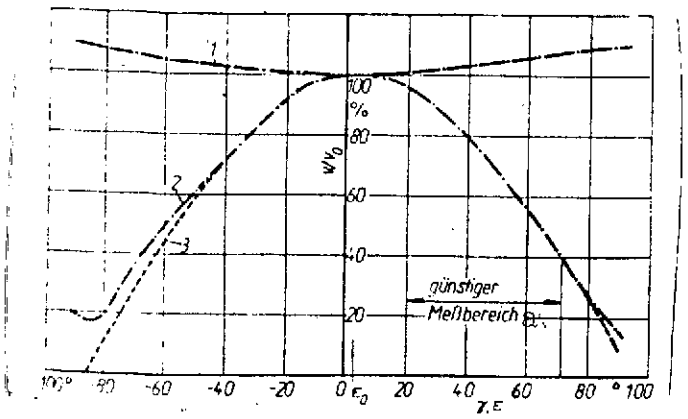

Fig. 11. Calibration curve for the hot-wire anemometer (cf. Fig. 12).
Curve 1: $v/v_0 = f(\gamma), \varepsilon = 0°$
Curve 2: $v/v_0 = f(\varepsilon), \gamma = 0°$
Curve 3; $v/v_0 = f[\cos(\varepsilon - \varepsilon_0)]$

Key: a. favorable measurement range

3.3 Recording the Velocity Distribution

For the measurements a system was developed, which, as already mentioned consists of a probe holder, transducer element and adjustment mechanism. The hot-wire anemometer can move by one or more divisions upon a cylinder section in the radial direction relative to the impeller. The thrust velocity is 1.5 mm/s maximum. The adjusting path of the probes is measured with digits in the moving system by impulses, which is directed outwards over slip rings and transformed electronically to a voltage proportional to the impulse number. The voltage is applied on the X-axis of an X,Y recording apparatus, on the Y-axis of which the velocity signal is given. An oscillascope was used as an X, Y recording apparatus. The velocity distribution was depicted upon this and it was photographed with a Polaroid Camera.

The hot-wire signal was translated from the rotating system with a mercury rotating transducer. This transducer, in which the electrical signal from a platinum-iridium axle rotating in a mercury bath was recorded upon a stationary contact met -- in view of its transition resistance for various numbers of revolutions -- the stringent requirements posed by the use of a constant resistance hot-wire anemometer. The maximum resistance variation in the rpm region of 0 to 3000 was ± 6mΩ. This yields an error in the velocity of at most ± 0.5%.

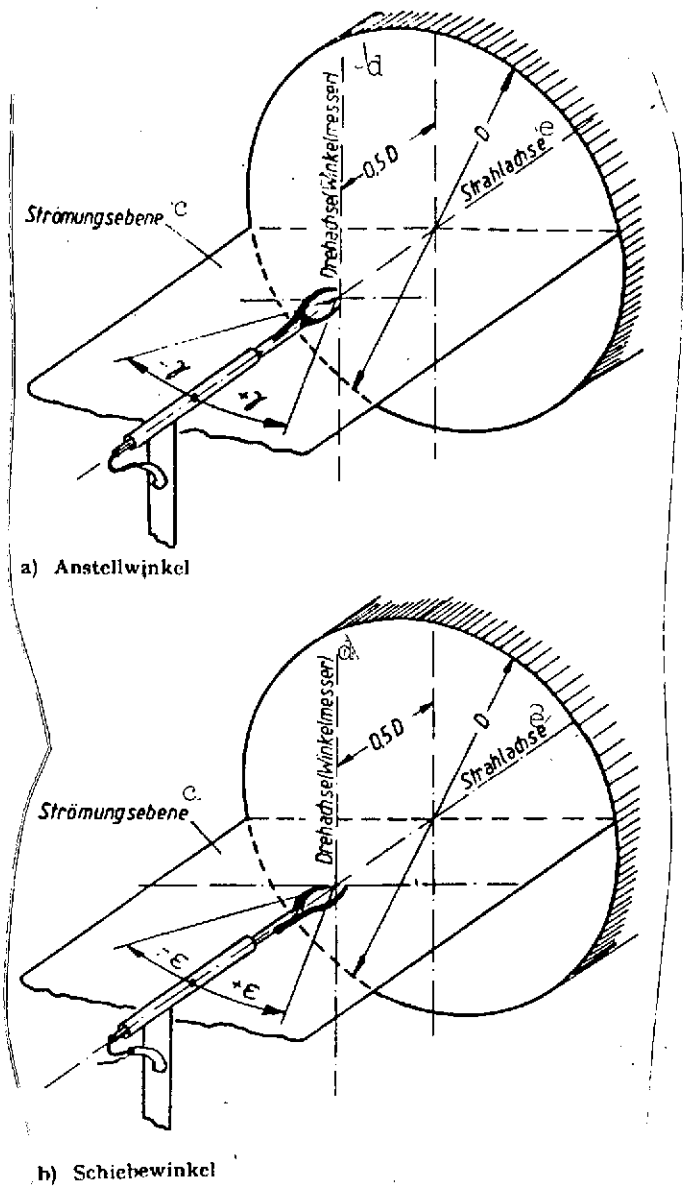

Fig. 12. Depiction of the flow angle of the hot-wire anemometer in a free-springing nappe(calibration).

Key: a. angle of incidence
b. angle of side slip
c. flow plane
d. rotation axes (angle measure)
e. nappe axis

The absolute velocity was measured in the same blade passage as the relative velocity. This was achieved by controlling the beginning of the recording with an external trigger signal. the recording was likewise photographically preserved.

4. Performance of the experiment

The effect of the clearance flow was investigated in the three operating conditions of the impeller shown in Fig. 6. Point 1 is an operating level of high capacity and small pressure increase, that is small blade load. At operating point 2 the greatest efficiency is achieved. Point 3 is an operating point near the limit of disruption of flow for strong thrusting of the capacity and great blade load.

In these three operating /39 conditions, the velocity field was measured with and without clearance flow. The three chosen operating points of the ventilator were so set for all measurements, that the flow

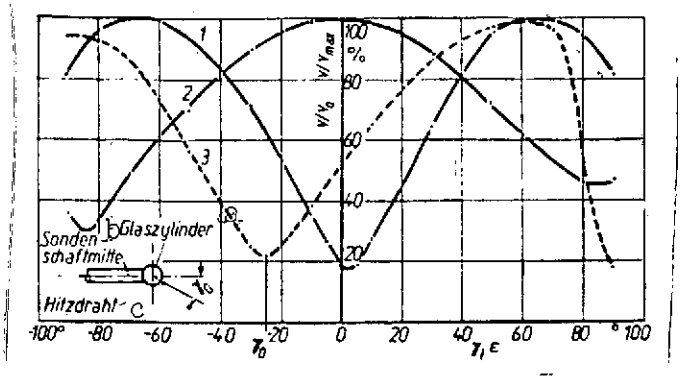

Fig. 13. Calibration curve for the hot-wire direction probe (cf. Fig. 12).
Curve 1: $v/v_{max} = f(\gamma)$, $\varepsilon = 0°$
Curve 2: $v/v_0 = f(\varepsilon)$, $\gamma = 0°$
Curve 3: $v/v_{max} = f(\gamma)$, $\varepsilon = 0°$

Key: a. glass cylinder
b. probe shaft middle
c. hot-wire

coefficient of the respective operating points remain constant according to Fig. 6. The impeller draws the same volume flow both with and without a clearance. This was determined because the flow conditions or the inlet triangles remain constant and the changes of the velocity field at the impeller discharge because of the clearance do not need to be attributed to varying flow conditions.

To ascertain the velocity field the velocity over a blade portion was measured (cf., e.g. Fig. 14) for seven ratios r/R = 0.647; 0.7; 0.8; 0.9; 0.94; 0;96 and 0;98. Since all blade passages had in the mean an equal flow through, as can be seen in Fig. 15 from the depiction of the absolute flow through all 12 passages, the investigation was only performed on one of the 12 blade passages.

For measurements without the impeller clearance the clearance between the impeller and the housing had to be closed without disturbing the flow in the blade passage which was to be measured. After a few pretests a simple strip of paper was shown to be a suitable sealant for the clearance between the impeller and the housing. It was pasted to the blade pressure side and along the housing wall (cf. Fig. 16). In order to prevent the paper strip from disturbing the flow in the passage under study it was attached to the suction side of the neighboring passage. There was no way to avoid the fact that with severe throttling the flow in this neighboring passage tended towards flow disruption. After the blade sealing the distribution of the velocity over all 12 blade passages was obtained with a stationary probe.

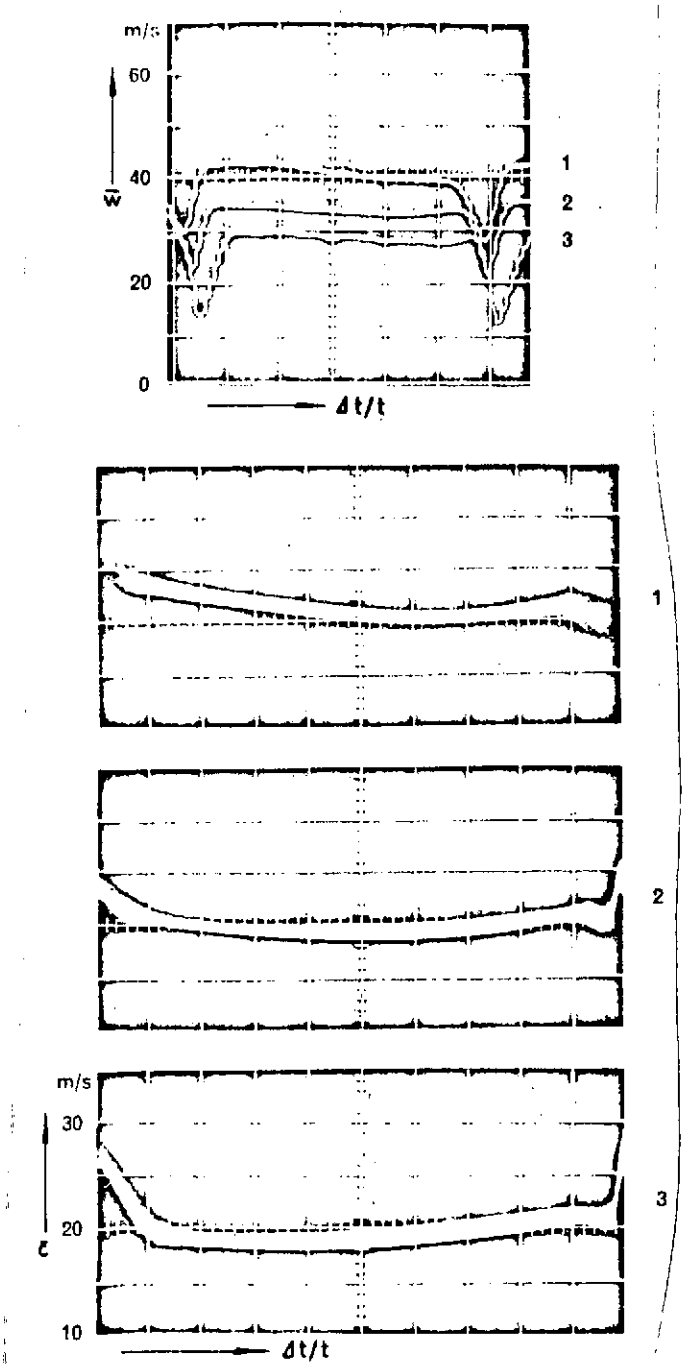

Fig. 14. Measurement values of the temporal median values of the relative velocity $\bar{w}$ and the absolute velocity $\bar{a}$ with the presence of a clearance between the impeller and the housing and r/R = 0.9 for the thrust conditions 1-3 (cf. Fig. 6) plotted against dimension lifts interval $\Delta t/t$ from the suction side (cf. Fig. 3).

Fig. 15b shows the course of the absolute velocity through the passages with a radial ratio of 0.96. It can be seen that the turbulence is stronger in the neighboring passage under very severe throttling (throttling position 3) in this outer blade region than in the other passages. These turbulence phenomena are typical for a beginning dissolution of the flow. The figure further shows that this disturbance in the neighboring passage does not have any effect upon the flow in the blade passage, in which the velocity field was measured.

5. Measurement Results

In Fig. 17 the course of the relative velocity with and without clearance flow is depicted for the radial ratios 0.94; 0.96 and 0.98. In these outer sections the velocity flows with and without clearance flow can be clearly differentiated.

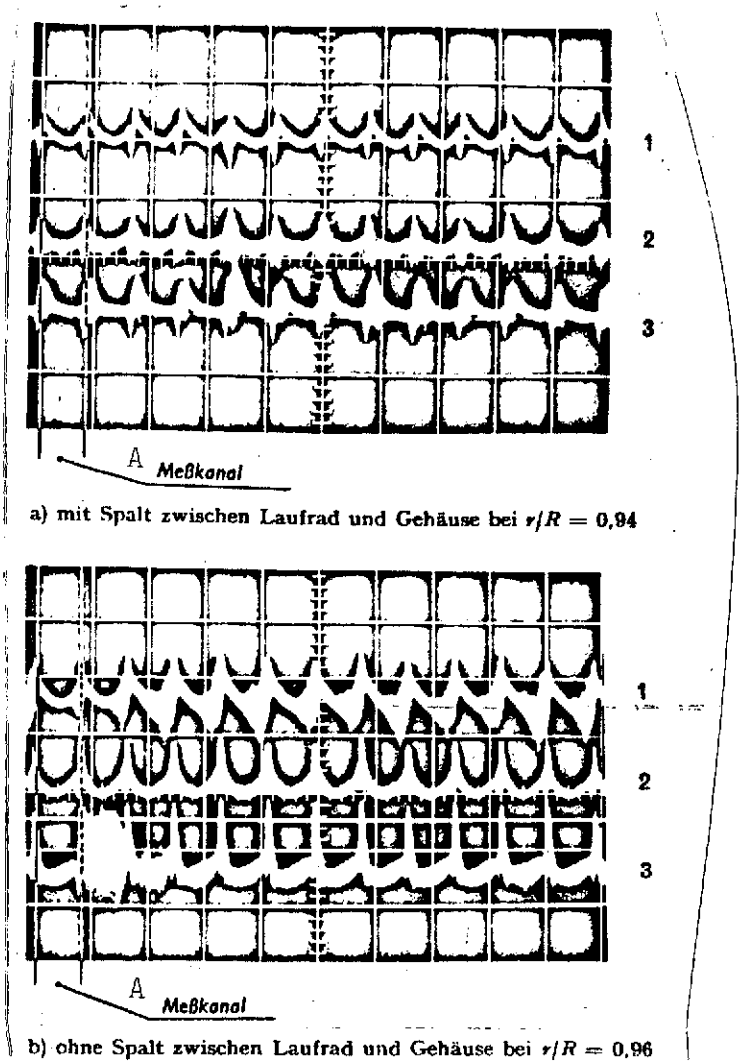

Fig. 15. Distribution of the absolute velocity over all 12 blade passages for the throttle positions 1 through 3 (cf. Fig. 6). a) with a clearance between the impeller and the housing at r/R = 0.94. b) without clearance between the impeller and the housing at r/R = 0.96.

Key: A. measurement passage

can be explained as follows:

The effect of a clearance can be seen in a type of velocity dip, which shifts from an unthrottled to a strongly throttled operating condition from the suction side to the pressure side. From the course of the velocities can be seen that even under strongly throttled conditions the velocities are relatively large on the suction side and that the flow has not been separated. This immediate effect upon the course of the velocity can be seen at approximately 80% of the blade height. If there is no clearance flow, then the velocity is very equally distributed to about 95% of the blade height. Then, however, -- in contrast to the case with a clearance -- the velocity /40 course changes decisively at the throttle positon 3. The velocity decreases sharply on the suction side, i.e. the flow is interrupted here. The fact that no interruption appears when a clearance is present at the operating point and that a dip in the velocity curve appears

The clearance flow, supported by the relative movement of the wall tears the boundary material from the suction side. At the throttle position 3, at which the blades are highly loaded there is a large pressure gradient between the pressure and suction sides of the blades created by a clearance flow from the blade pressure side to the blade suction side with corresponding kinetic energy. For other throttle positions 1 and 2 this pressure ratio must be smaller, since the blade load is not as great in these cases. A smaller impulse of the clearance flow, however, corresponds to the smaller pressure gradient.

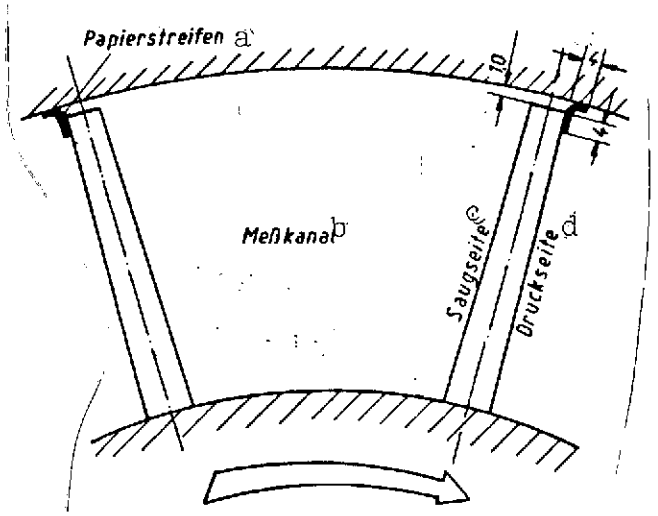

Fig. 16. Schematic representation of the closing of the clearance between the impeller and the housing wall.

Key: a. paper strip
b. measurement passage
c. suction side
d. pressure side

On the other hand, there is a pressure field in the blade passage which causes a flow from the pressure side of the blade to the suction side on the boundary layer at the side wall. With increasing blade depth it becomes weaker transverse to the blade passage. The medium flowing from the clearance must, therefore, flow against this pressure field. It is supported by the relative movement of the housing wall, which brings about a certain tow effect. Therefore, the more energetic clearance flow can, under heavy throttling, flow against the pressure field and finally reach to the pressure side of the opposing blade. At the same time the clearance flow pushes the boundary layer material at the housing wall and the blade suction side away from the suction side and becomes mixed with /41 this. A region with an energy poor flow comes about, which appears as a dip in the velocity curve.

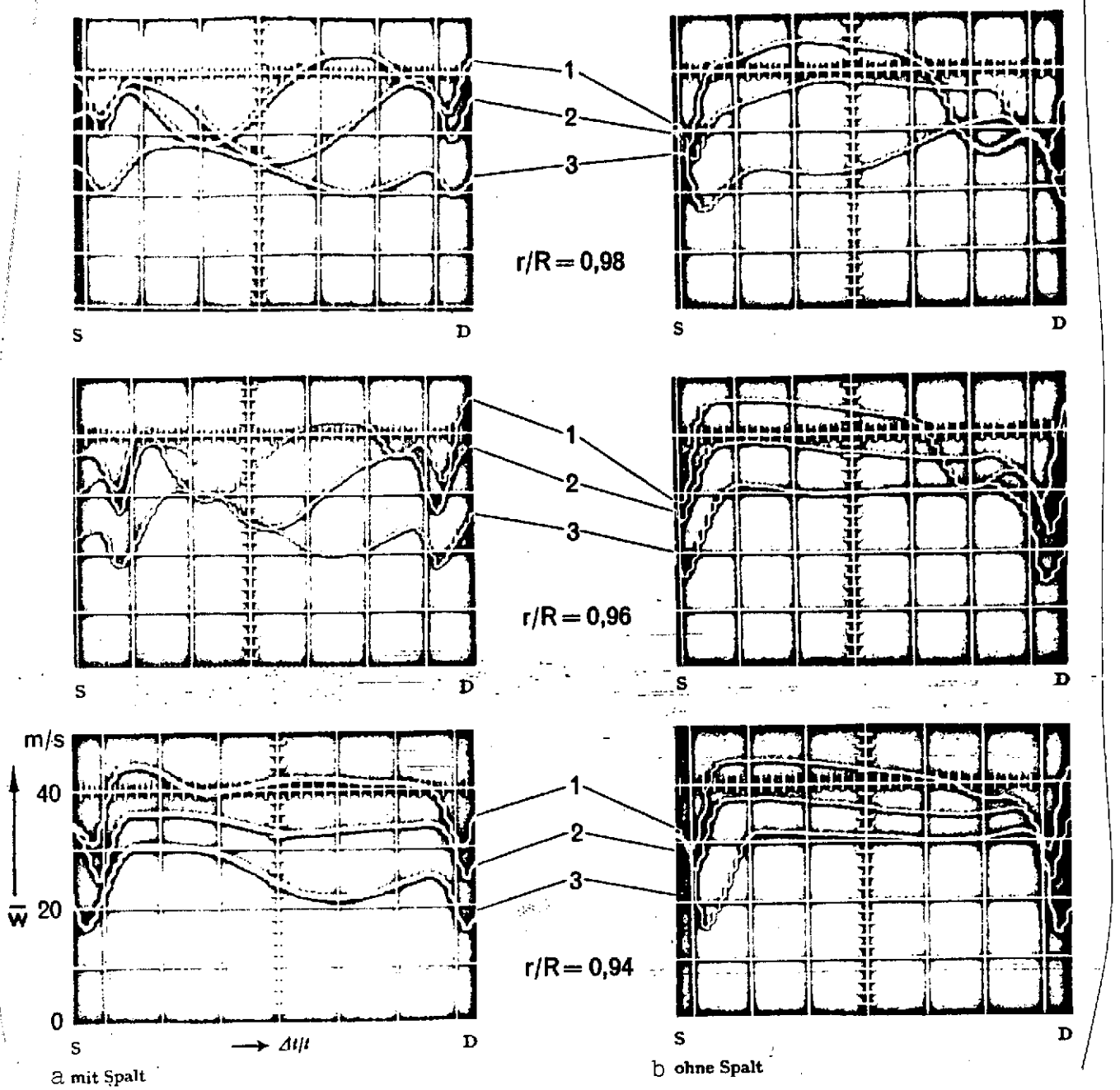

Fig. 17. Relative velocity $\bar{w}$ plotted against dimensionless interval $\Delta t/t$ of the suction side with and without clearance between the impeller and the housing for various ratios r/R and for the throttle positions 1 through 3 (cf. Fig. 6). S = suction side, D = pressure side.

Key: a. with clearance
b. without clearance

In the region of the suction side in which the energy poor flow medium is sucked up by the clearance flow material with greater

velocity can flow from the undisturbed flow. This causes high-flow velocities to appear on the blade suction side as shown in Fig. 17. These observations were made on a stationary blade by R. C. Dean Jr. [5] and A. Fritzsche [6].

The measurements of the velocity distribution in the grade passage (Fig. 18a through 18c) show the properties described above even clearer. For the throttle position 3 (Fig. 18a) a dip in the velocity curve can be seen for 10% blade depth in the proximity of the suction side. The clearance flow begins to enter the boundary layer on the side wall here. At 30% blade depth the clearance flow has begun to mix with the side wall and blade boundary layer to create a region of low energy flow on the suction side and they begin to move towards the blade pressure side together. In this liberated area material flows along the blade suction side. Through a kind of sucking away of the boundary level the flow is established despite the great blade load near the limit of flow disruption, at which the flow on the suction side must be interrupted at about 1/3 of the blade depth.

The velocity distribution given for the throttle positions 1 and 2 can also be explained by the flow processes described for throttle position 3. An even smaller pressure gradient between the blade pressure and the blade suction sides is present for the clearance flow from throttle position 2 to throttle position 1 in order to maintain the necessary flow energy with which it can flow against the pressure field in the blade passage. Fig. 18a shows that at these throttle positions the clearance flow changes the velocity curve in the blade passage first at $\Delta\ell/\ell = 0.3$ ($\Delta\ell$ = interval from the blade leading edge). The action, however, takes place so that immediately on the blade suction side boundary layer material is pushed off and space is made for the medium with greater flow velocity. For the throttle position 2 the clearance flow is able to push the boundary layer material up to the blade and in the blade passage center. Since the flow through the blade passage is usually a blade flow, this flow is

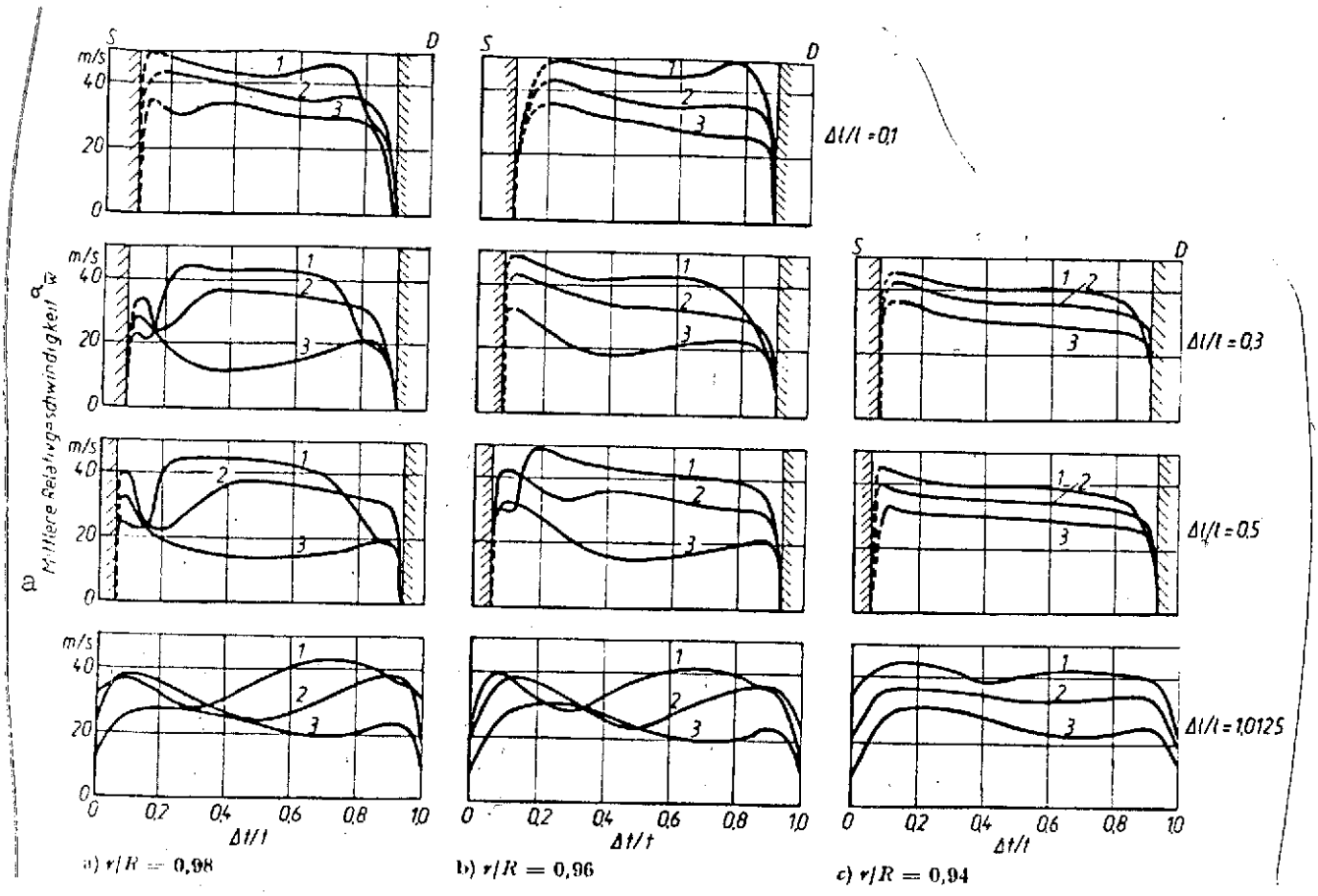

Fig. 18. Relative velocity $\bar{w}$ plotted against dimensionless interval $\Delta t/t$ (cf. Fig. 3) for various dimensionless intervals $\Delta \ell/\ell$ of the blade leading edge (cf. Fig. 3) and the throttle position 1 through 3 (cf. Fig. 6). S = suction side, D = pressure side.

Key: a. median relative velocity

especially sensitive to disturbances. A disturbance in the velocity curve, such as that caused by the clearance flow increases in the course of the grid flow-through. This can be seen clearly from Fig. 18a through 18c as well as Fig. 17.

For the throttle position 1 and expansion of the boundary layer on the pressure side can be detected, which is present both with and without a clearance and, therefore, is not caused by the clearance or

clearance closing. This expansion cannot be explained by the tow /42
effect of the wall or a kind of abrasion of the wall boundary layer in which the blades collect boundary material on the pressure side and a decrease in velocity results. If the first or second effect was the primary cause, then they must also appear for the other throttle positions in the velocity curve. The cause must be seen if an unfavorable incident flow upon the blades in these outer sections. Since the approaching boundary layer of the housing wall is relatively thin the cylinder section r/R = 0.98 lies outside of the boundary layer (cf. Fig. 19). The flow reaches the blades with a negative angle of incidence, as can be seen in Fig. 20, so that a disturbance upon the pressure side can appear in the form of separation bubbles, which lead to the thickening of the boundary layer on the pressure side. In Fig. 18a to 18c it can be seen that with the radial ratios r/R = 0.98 (Fig. 18a) such a disturbance in the boundary layer is already present, which increases in the flow direction and points to this property. For the radial ratio r/R = 0.96 (Fig. 18b) the disturbance could not be detected in the forward blade section. On the other hand, it is strongly present at the end of the blade passage. For r/R = 0.94 it cannot be found at all (Fig. 18c). The fact that the tow effect on the housing wall for the thin boundary layer on the housing wall before the impeller contributes to a certain degree to the flow process on the pressure side can be clearly seen from the flow line within and without the boundary layer as shown in the schematically depicted processes in Fig. 21a. For the throttle 1 the main flow in the blade passage is only slightly deflected. Only a weak secondary flow appears on the pressure and suction side. The flow lines within the boundary layer on the side wall must, however, be strongly deflected in order to proceed in the direction of the main flow upon discharge from the blade cascades. It is supported by the secondary flow. The relative movement of the housing wall and the clearance flow work against the secondary flow. Since the secondary flow is only slightly intensified the flow within the boundary

layer does not receive the necessary support from it and is not deflected against the tow effect of the housing wall and the clearance flow (cf. Fig. 21a). The boundary layer material reaches the pressure side and increases the disturbance already present.

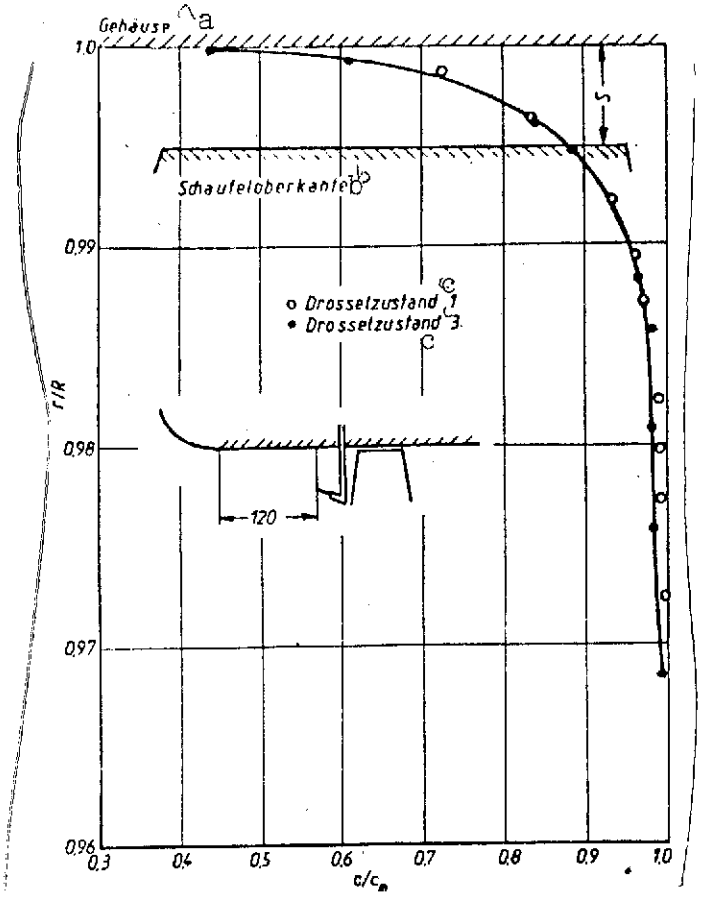

Fig. 19. Course of the boundary layer on the housing wall for the impeller. c = absolute velocity, c_m = median absolute velocity from volume flow/surface, s = clearance with

Key: a. housing
b. blade upper edge
c. throttle position

If the velocity curves in Fig. 17 for the case without a clearance are compared, it can be seen that the expansion of the boundary layer at the end of the blade passage is greater and can still be seen at r/R = 0.94. More material with lower flow energy collects here than with the presence of a clearance. This can be explained by noting that in this case no material can flow to the blade suction side.

With increasing throttling the flow direction of the primary flow nears that of the boundary layer. The deflection differences of the flow lines becomes smaller and the blades are flowed against with a positive angle of incidence outside of the boundary layer (Fig. 20). At the same time the greater deflection of the main flow /43 causes a larger pressure gradient transverse to the flow, which causes a more intensive secondary flow. The flow lines within the boundary layer are now more strongly deflected and the boundary layer material of the side wall flows more

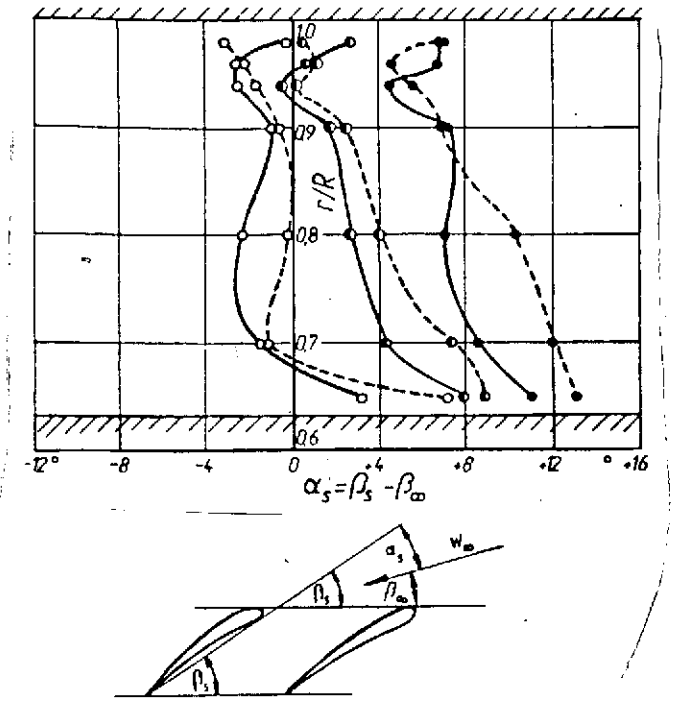

Fig. 20. Course of the angle of incidence $\alpha_s = \beta_s - \beta_\infty$ (cf. Fig 3) in the radial direction for the throttle positions 1 through 3 (cf. Fig. 6) with and without a clearance between the impeller and the housing

_____ with clearance,

_ _ _ _ _ _ _ without clearance

symbol	○	◐	●
throttle position	1	2	3

and more from the pressure side to the suction side. As, however, was explained above, it is slowed by the opposing clearance flow and the flow process described comes about.

In Fig. 21b, as in 21a, the assumed flow lines within and without the boundary layer are depicted for the case in which no clearance is present. The same considerations apply here. The clearance flow, however, is not present to counteract the secondary flow.

The tow effect of the housing wall alone can overcome the secondary flow only at throttle position 1. With increasing throttling its effect upon the secondary flow diminishes. The boundary layer material of the housing wall reaches the suction side more and more, thickens the boundary layer there and leads to the disruption of the flow. In Fig. 17 the disrupted flow at throttle position 3 and r/R = 0.98 can be recognized by the significantly lower velocity on the suction side. Even at throttle position 2 it can be clearly seen that the velocity decreases towards the suction side.

The immediate effect of the clearance flow is noticeable above approximately 20% of the blade height. The area as far as the hub is indirectly affected by this disturbed flow region, in that the circumferential components, axial components and the work conversion are changed in the mean. In order to show these indirect effects

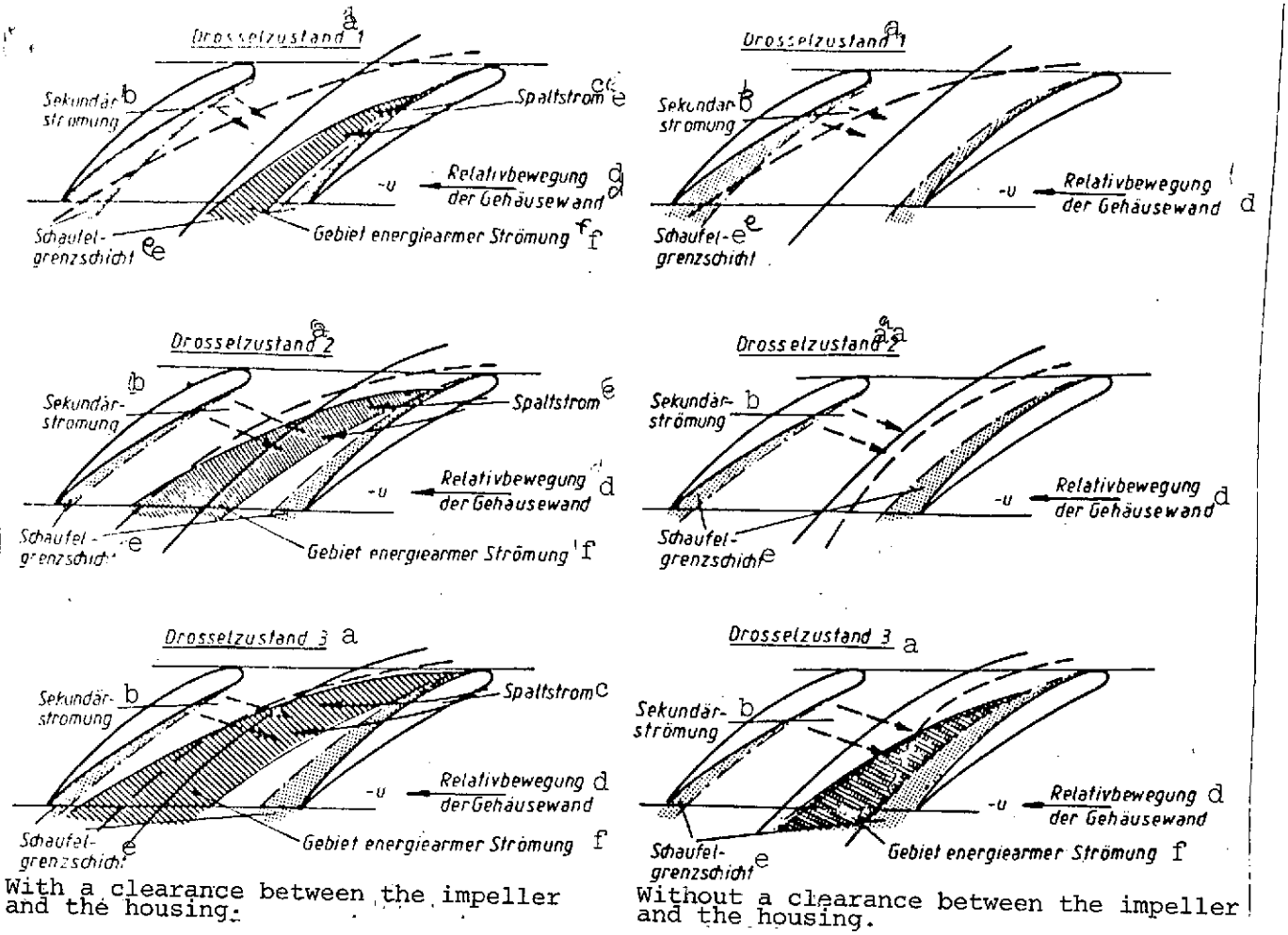

Fig. 21. Schematic representation of the flow line deflection within and without the boundary layer at the housing wall.
_____ flow line outside of the boundary layer,
_ _ _ _ _ _ _ flow line within the boundary layer.

Key. a. throttle position
b. secondary flow
c. clearance flow
d. relative movement of the housing wall
e. blade boundary layer
f. region of energy poor flow

representative mean values of a rotationally symmetrical velocity field for the individual cylinder sections or formed as follows:

The mean value of the axial components $C_{x,m}$ related to the circumferential velocity of the impeller at the outer radius $C_{x,m} = c_{x,m}/u_a$ is given from

$$E = (r/R)\int_0^1 C_u C_x \, d\left(\frac{\Delta t}{t}\right)$$

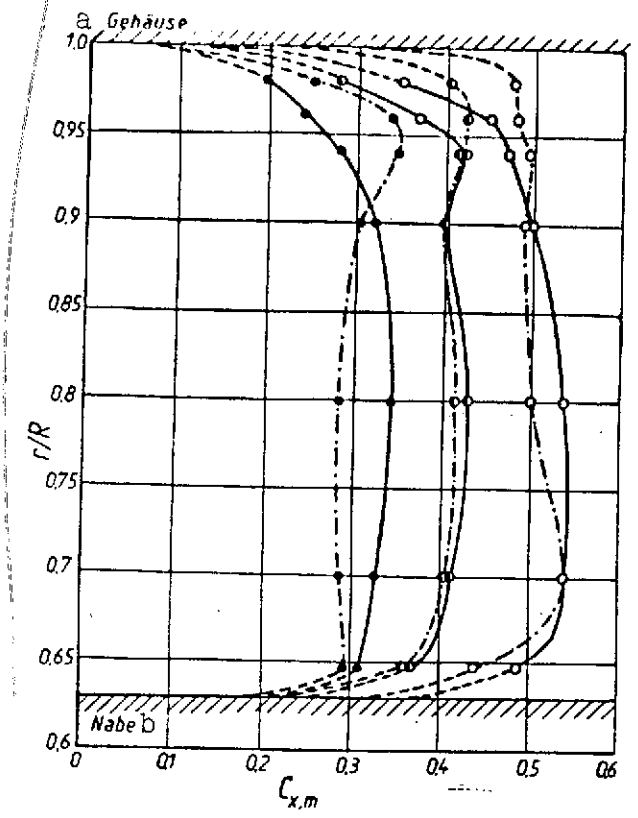

Fig. 22. Distribution of the mediated axial components $C_{x,m}$ of the absolute velocity over the blade passage height for the throttle positions 1 through 3 (cf. Fig. 6) with and without clearance between the impeller and the housing
_____ with clearance
_ _ _ _ without clearance

symbol	○	◐	●
throttle position	1	2	3

Key: a. housing
b. hub

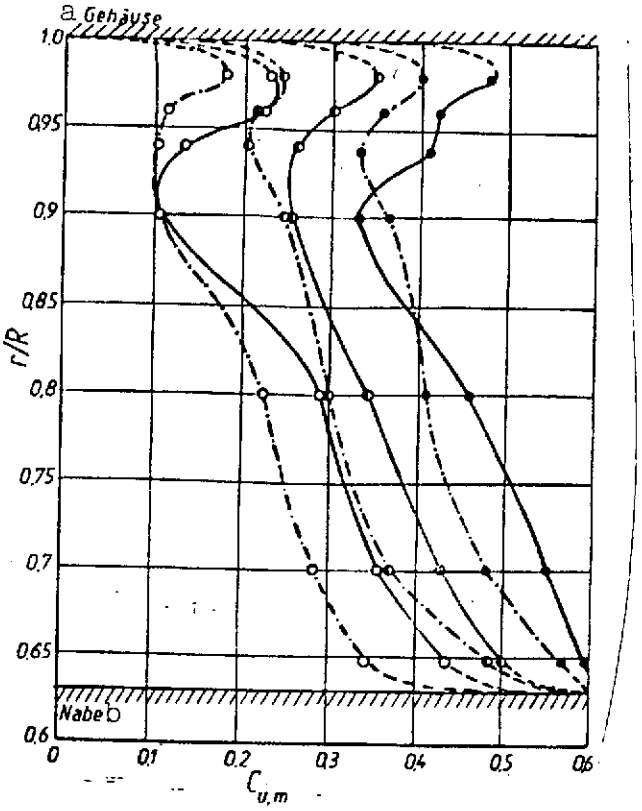

Fig. 23. Distribution of the mediated radial components $C_{u,m}$ of the absolute velocity over the blade passage height for the throttle positions 1 through 3 (cf. Fig. 6) with and without a clearance between the impeller and the housing
_____ with clearance,
_ _ _ _ _ without clearance

symbol	○	◐	●
throttle position	1	2	3

Key: a. housing
b. hub

whereby $\Delta t/t$ is the given dimensionless distance from the blade's suction side.

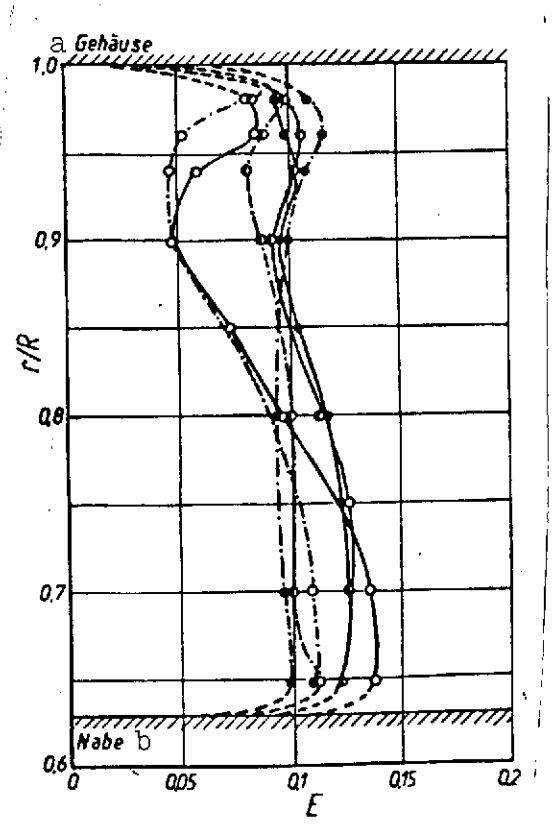

Fig. 24. Characteristic value of the work conversion

$$E = (r/R)\int_0^1 C_u C_x \, d\left(\frac{\Delta t}{t}\right)$$

over the blade passage height for the throttle positions 1 through 3 (cf. Fig. 6) with and without a clearance between the impeller and the housing

———— with clearance
– – – – – without clearance

symbol	○	◐	●
throttle position	1	2	3

Key: a. housing
b. hub

The circumferential components of the absolute flow are found from the equation

wherein $C_x = \bar{c}_x/u_a$ and $C_u = \bar{c}_u/u_a$.

In the Figs. 22 and 23 the distribution of the mediated values over the blade height is/44 depicted. The effects of the clearance flow upon the total velocity curve over the blade height can be clearly seen. Since the clearance flow causes a thickening of the side wall boundary layer at the blade tips, the axial components of the flow up to the hub are greater than without a clearance. The circumferential components of the absolute flow are also greater. In Fig. 24, the energy flow distribution given from the equation

is depicted over the blade height. It corresponds to the work conversion of the impeller.